biosensors

MDPI

Article

Comparative Colorimetric Sensor Based on Bi-Phase γ-/α-Fe_2O_3 and γ-/α-Fe_2O_3/ZnO Nanoparticles for Lactate Detection

Ricardo A. Escalona-Villalpando [1], Karen Viveros-Palma [1], Fabiola I. Espinosa-Lagunes [2], José A. Rodríguez-Morales [1], Luis G. Arriaga [2], Florika C. Macazo [3], Shelley D. Minteer [3] and Janet Ledesma-García [1,*]

[1] División de Investigación y Posgrado, Facultad de Ingeniería, Universidad Autónoma de Querétaro, Santiago de Querétaro 76010, Mexico
[2] Centro de Investigación y Desarrollo Tecnológico en Electroquímica, Pedro Escobedo 76703, Mexico
[3] Department of Chemistry, University of Utah, 315 South 1400 East, Salt Lake City, UT 84112, USA
* Correspondence: janet.ledesma@uaq.mx

Abstract: This work reports on Fe_2O_3 and ZnO materials for lactate quantification. In the synthesis, the bi-phase γ-/α-Fe_2O_3 and γ-/α-Fe_2O_3/ZnO nanoparticles (NPs) were obtained for their application in a lactate colorimetric sensor. The crystalline phases of the NPs were analyzed by XRD and XPS techniques. S/TEM images showed spheres with an 18 nm average and a needle length from 125 to 330 nm and 18 nm in diameter. The γ-/α-Fe_2O_3 and γ-/α-Fe_2O_3/ZnO were used to evaluate the catalytic activity of peroxidase with the substrate 3,3,5,5-tetramethylbenzidine (TMB), obtaining a linear range of 50 to 1000 μM for both NPs, and a 4.3 μM and 9.4 μM limit of detection (LOD), respectively. Moreover, γ-/α-Fe_2O_3 and γ-/α-Fe_2O_3/ZnO/lactate oxidase with TMB assays in the presence of lactate showed a linear range of 50 to 1000 μM, and both NPs proved to be highly selective in the presence of interferents. Finally, a sample of human serum was also tested, and the results were compared with a commercial lactometer. The use of ZnO with Fe_2O_3 achieved a greater response toward lactate oxidation reaction, and has implementation in a lactate colorimetric sensor using materials that are economically accessible and easy to synthesize.

Keywords: lactate colorimetric sensor; bi-phase γ-/α-Fe_2O_3; peroxidase-like activity; lactate oxidation; bi-phase γ-/α-Fe_2O_3/ZnO

Citation: Escalona-Villalpando, R.A.; Viveros-Palma, K.; Espinosa-Lagunes, F.I.; Rodríguez-Morales, J.A.; Arriaga, L.G.; Macazo, F.C.; Minteer, S.D.; Ledesma-García, J. Comparative Colorimetric Sensor Based on Bi-Phase γ-/α-Fe_2O_3 and γ-/α-Fe_2O_3/ZnO Nanoparticles for Lactate Detection. *Biosensors* **2022**, *12*, 1025. https://doi.org/10.3390/bios12111025

Received: 12 October 2022
Accepted: 9 November 2022
Published: 16 November 2022

1. Introduction

Lactate is a metabolite resulting from the anaerobic process of the respiratory chain in cells. Its quantifying is related to clinical diagnosis, the study of metabolic diseases, and continuous monitoring in sports medicine, trauma, and the food industry [1]. Lactate concentration is usually determined by HPLC, fluorometry, colorimetric tests [2], chemiluminescence, magnetic resonance spectroscopy, or electrochemical methods [3]. Each technique has certain advantages; although in some cases, the equipment is complex and expensive. In the case of colorimetric techniques, they are among the most required, because they are simpler and the equipment is economically accessible, but sometimes, its low sensitivity, quantification ranges, and limits of detection are parameters that are in constant investigation and improvement [4,5]. Conventionally, lactate has been quantified in blood or serum at concentrations of 0.5–2.5 mM, but this technique has the drawback that it is invasive to obtain the sample. Therefore, the trend in colorimetric quantification of lactate has been focused on sweat with concentration ranges from 15 to over 65 mM [6], although not all already reported sensors reach these quantifiable values [7]. Another of the biological fluids where the lactate could be measurable is the saliva, where the concentration varies between 0.11 to 0.56 mM, so it can be challenging to quantify it by colorimetric methods [8].

For the colorimetric quantification of lactate, the lactate oxidase enzyme (LOx) is usually used, where pyruvate and hydrogen peroxide (H_2O_2) result as secondary products. From this reaction, H_2O_2 is used as a substrate to react with a metal or metallic oxide with peroxidase-like activity and a chromogenic substance such as TMB that can be measured by UV-Vis spectroscopy [4]. Peroxidase-like iron oxides or iron-modified oxides have preferably been used due to their catalytic activity that depends on their intrinsic properties. These materials are also economically more viable compared to precious metals such as gold [9,10] or silver [11,12]. The peroxidase-like activity of Fe_3O_4 followed a trend of spheres > triangular plates > octahedral [13], with a smaller size to 30 nm [14,15] that has been published. Fe_2O_3 has also been reported from alpha and gamma phases, although with a low peroxidase-like activity for this last phase [16,17]. Binding with another material such as CeO_2, CuO, Co_3O_4, V_2O_5, and $ZnFe_2O_4$ [18] can increase the catalytic activity. In addition, using other types of oxides, such as SiO_2 or ZnO, facilitates a union with proteins improving mechanical and photovoltaic properties [19,20].

In this work, the synthesis of Fe_2O_3 and Fe_2O_3/ZnO by a simple and controlled precipitation method that could obtain the phases γ-/α-Fe_2O_3 and γ-/α-Fe_2O_3/ZnO is presented. Both materials were evaluated as peroxidase mimics through the catalytic oxidation of hydrogen peroxide. TMB concentration, wavelength, and H_2O_2 concentrations were standardized. Subsequently, both NPs were used to quantify lactate with the LOx enzyme (Scheme 1), which has been poorly studied compared to other molecules such as glucose [21]. Therefore, we report the modification of Fe_2O_3 with ZnO in order to improve the stability of the enzyme and catalytic activity through the peroxidase activity of Fe_2O_3 used as a colorimetric lactate biosensor.

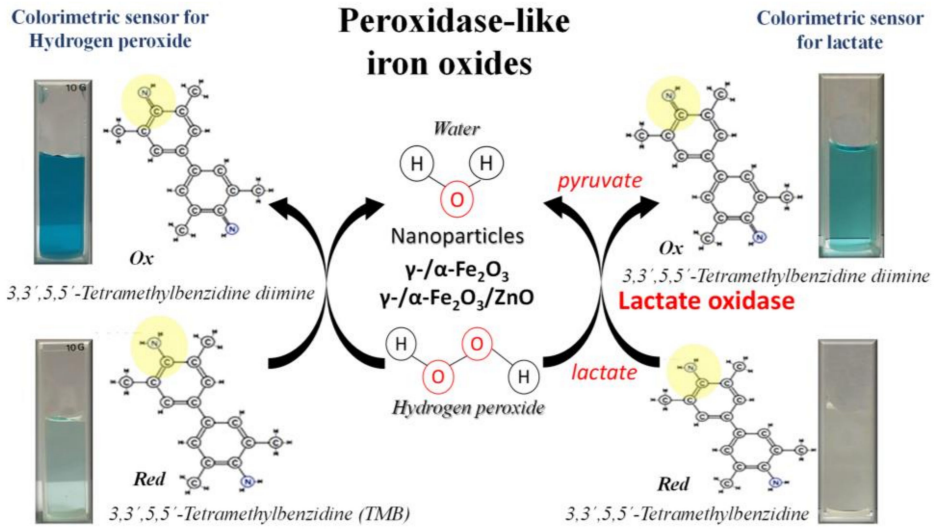

Scheme 1. Reaction between TMB with γ-/α-Fe_2O_3 or γ-/α-Fe_2O_3/ZnO in the presence of H_2O_2 (**left**) and H_2O_2 generated from lactate oxidation by LOx (**right**).

2. Materials and Methods

2.1. Materials

All used reagents are analytical grade from commercial sources. $FeCl_3 \cdot 6H_2O$, TMB, H_2O_2 (30%), NaOH, LOx from Aeroccoccus viridans, $Zn(O_2CH_3)_2 \cdot 2H_2O$, anhydrous sodium acetate, acetic acid, 3,3,5,5-tetramethylbenzidine TMB, and dimethyl sulfoxide (DMSO) were obtained from Sigma-Aldrich. Phosphate buffer solution (PBS) was prepared using Na_2HPO_4 and KH_2PO_4 (pH 7.4) from J.T. Baker. Acetate buffer solution (HAc-NaAc) was prepared from acetic acid and sodium acetate (pH 5) obtained from J. T. Baker. All aqueous solutions were prepared using deionized water DI ($\sigma \geq 18$ MΩ cm).

2.2. Synthesis of Fe_2O_3 and Fe_2O_3/ZnO

Briefly, Fe_2O_3 preparation consisted of $Fe_2Cl_3 \cdot 6H_2O$ salt (1 mol) in DI water (10 mL) in an ultrasonic bath for 30 min, keeping the temperature below 25 °C. Subsequently, 1.5 M NaOH (25 mL) was added slowly using a programmed injection pump for 1 h. Finally, the solution was maintained at 50 °C for 3 h under constant stirring. The precipitate was collected and washed several times with DI. The product was dried in an oven at 100° C for 24 h and then calcined at 500 °C during 4 h. For Fe_2O_3/ZnO nanoparticles, the synthesis procedure is as follows: 3 M NaOH (10 mL) was added by drop for 30 min using an injection pump to 1 mol $Zn(O_2CH_3)_2 \cdot 2H_2O$ in DI (10 mL) under constant sonication. At the same time, 1 mol $Fe_2Cl_3 \cdot 6H_2O$ dissolved in 10 mL of DI and 10 mL 3 M NaOH was added by drop to the previous solution (injection pump) over a period of 30 min. Finally, the mixture was heated at 50 °C for 3 h. After that time, the precipitate was filtered and dried at 100 °C for 24 h and then calcined at 500 °C for 4 h in ramps with a temperature increase of 50 °C every 30 min.

2.3. Peroxidase-like Activity Measurements

The peroxidase-like behavior of the γ-/α-Fe_2O_3 and γ-/α-Fe_2O_3/ZnO NPs was analyzed spectrophotometrically at 653 nm through the H_2O_2 oxidation in the presence of TMB. The catalytic activity of γ-/α-Fe_2O_3 and γ-/α-Fe_2O_3/ZnO NPs toward TMB oxidation was studied using 5 mg mL^{-1} of NP's (20 µL), 500 µM TMB in DMSO (30 µL), NaHOAc buffer (0.01 M, pH 4.0, 1.9 mL), and 30% H_2O_2 (30 µL). The wavelength was selected from a measurement sweep between 400 to 800 nm in the presence of 500 µM H_2O_2 using a UV-Vis spectrophotometer. The concentrations of oxidized TMB were quantified by UV–vis absorption using $\varepsilon = 3.9 \times 10^4$ M^{-1} cm^{-1} as the molar extinction coefficient [19]. The kinetic analysis using TMB as the substrate was performed varying the concentrations in the absence of TMB until 1500 µM. Similarly, the kinetics analysis with H_2O_2 was performed by varying the concentrations (0, 1, 5, 10, 50, 100, 250, 500, 750, 1000, and 1500 µM) for 10 min. The Michaelis–Menten constant was calculated using Lineweaver–Burk plots, $1/\nu = Km/Vm\ (1/[S] + 1/Km)$; ν is the initial velocity, Vm is the maximal reaction velocity, [S] is the concentration of the substrate, and Km is the Michaelis constant. The determination of each sample was repeated three times.

2.4. Colorimetric Measurement of Lactate Using γ-/α-Fe_2O_3 and γ-/α-Fe_2O_3/ZnO NPs

Lactate detection was performed using 40 µL of LOx (100 U mL^{-1}) in phosphate buffer solution (0.01 M PBS pH 7) using 200 µL of different lactate concentrations (0, 5, 10, 50, 100, 300, 500, 800, 1000, 3000, and 5000 µM). The solutions were incubated at 37 °C for 30 min. Later, 30 µL of TMB (500 µM), 20 µL of γ-/α-Fe_2O_3 and γ-/α-Fe_2O_3/ZnO (5 mg mL^{-1}) NPs and acetate buffer (pH 4) were added into the LOx-lactate solution (final volume: 2 mL) and the solution was incubated at 37 °C for 15 min. Finally, the resulting solution was separated from the NPs by decanting, and then the absorbance was measured at 653 nm. The limit of detection (LOD) was calculated considering 3 σ/S; σ is the standard deviation of the blank signal and S the sensitivity obtained from the slope of the calibration cure, whereas the limit of quantification (LOQ) was calculated from 10 σ/S. This same calculation was used for peroxidase-like activity measurements.

2.5. Colorimetric Evaluation of Lactate Using γ-/α-Fe_2O_3 and γ-/α-Fe_2O_3/ZnO in the Presence of Interferents and Real Samples

To evaluate the selectivity of the colorimetric lactate sensor, 1 mM lactate was used in the presence of 0.5 mM interferents separately as dopamine (DA), ascorbic acid (AA), uric acid (UA), glucose (Glu), urea, Ca^{2+}, and Fe^{3+}. Each interferent with each NP was performed in triplicate way, reporting the error bars as standard deviation. The evaluation was made in a real sample following the methodology presented in Section 2.4, but instead using 200 µL of human serum obtained from blood by venipuncture in a vacutainer(R) tube with anticoagulant from six healthy volunteers. To verify the calculated lactate

concentration, an Accutrend® Plus brand commercial lactometer (Roche, Basel, Switzerland) was used.

2.6. Characterization of γ-/α-Fe_2O_3 and γ-/α-Fe_2O_3/ZnO NPs

The crystal structure of the NPs was determined by an X-ray diffraction (XRD) measurement that was carried out by a Bruker X-ray diffractometer model PW3710 radiation CuK (alpha 1) (wavelength: 1.54 Å). X-ray photoelectron spectroscopy (XPS) analysis was performed using an instrument (Monochromatic Magics Thermo Scientifics, model K-Alpha+) in conditions of v = 1 scan/min, t = 20.5 s and CAE = 20. A L6S/L6 UV-Vis spectrophotometer was used to measure absorbance.

3. Results and Discussion

3.1. Characterization of γ-/α-Fe_2O_3 and γ-/α-Fe_2O_3/ZnO

From XRD analysis, the crystalline phase and size of the Fe_2O_3 and Fe_2O_3/ZnO nanoparticles were estimated. Analyzing the peaks belonging to the Fe_2O_3 (Figure 1), the diffraction peaks match the standard rhomboeric pattern, having the characteristics (012), (104), (110), (113), (024), (116), (214), (300), (119), and (220) planes of α-Fe_2O_3 (hematite), and the displaced peaks of planes (220), (311), (400), (422), and (511), which correspond to γ-Fe_2O_3 (maghemite), which suggests that a bi-phase γ-/α-Fe_2O_3 is formed. The result is consistent with the values already reported (JCPDS: 033-0664 and JCPDS: 04-0755). The formation of the bi-phase γ-/α-Fe_2O_3, according to other authors, can be be attributed to the synthesis and calcination method; also, the data processing was performed using a detailed analysis by DIFRAC EVA software (2.0) [22,23]. For Fe_2O_3/ZnO-based materials, the diffraction patterns attributed to α-Fe_2O_3 can be observed according to JCPDS: 033-0664, whereas other well-defined diffraction peaks corresponding to ZnO, assigned (100), (002), (101), (102), (110), (103), (112), and (201), were indicated, which correspond to JCPDS 36-1451 [24]. The Debye–Scherrer equation ($D = \kappa \lambda / \beta \cos \theta$) was used to estimate the size of the crystalline particles, where D is the crystal size in nm, λ is the X-ray wavelength (0.15406 nm), β is full-width at half-maximum of the peak, θ is the corresponding Bragg diffraction angle, and k is a constant (0.89) [25]. By consideration of the most representative peaks of each material, a particle size of 15 and 28.6 nm was calculated for γ-/α-Fe_2O_3 and γ-/α-Fe_2O_3/ZnO, respectively.

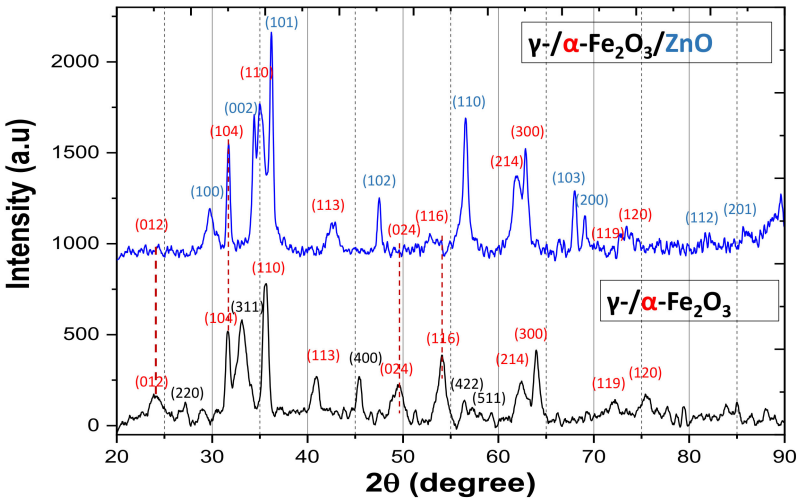

Figure 1. XRD patterns of the γ-/α-Fe_2O_3 (**down**) and γ-/α-Fe_2O_3/ZnO (**up**) nanoparticles.

XPS analysis of γ-/α-Fe_2O_3 (Figure 2A) shows a first fine scan of Fe 2p, observing the binding energy of the electrons given in $2p^{3/2}$, $2p^{1/2}$ in the bands 711.45 eV and 734.41 eV, respectively [26]; the separation of the 2p doublet is 14.0 eV [27]. Specifically, the adjustment peaks that are located in the binding energies of 720.3, 724.2, 733.6, and 735.5 eV correspond

to the tetrahedral Fe $2p^{3/2}$, octahedral Fe $2p^{3/2}$ structure, and the Fe $2p^{1/2}$ satellite structure, whereas in the energies 711.3, 713.2, 718.6, and 725.5 eV, there is a signal shift observed, which indicates a normal state of Fe^{3+} in the two samples [28]. In the analysis of γ-/α-Fe_2O_3/ZnO (Figure 2B), a second scan of Zn 2p was made, showing the peaks in the energy band 1022.1 and 1045.0 eV, which are attributed $2p^{3/2}$ and Zn $2p^{1/2}$, respectively, indicating that the oxidation state of Zn is 2^+, whereas those located at 1021.4 and 1044.4 eV are attributed to Zn in the ZnO phase, as shown in the Supplementary Materials Figure S1C [29]. By the analysis of the material based on γ-/α-Fe_2O_3/ZnO (Figure S1), it was found that the corresponding signals for γ-Fe_2O_3 and α-Fe_2O_3 at 532.5 eV can be attributed to a chemisorption process, whereas the peaks located at 560.5 and 584.5 eV are associated with the oxygen of the network in the framework of metal oxides (Zn/Fe) [27]. In addition, the atomic percentages of Zn, Fe, and O were calculated and adjusted to the fine-scan spectra Zn, Fe, and O, showing the Zn/Fe/O ratio of 1:2:4 in Table S1.

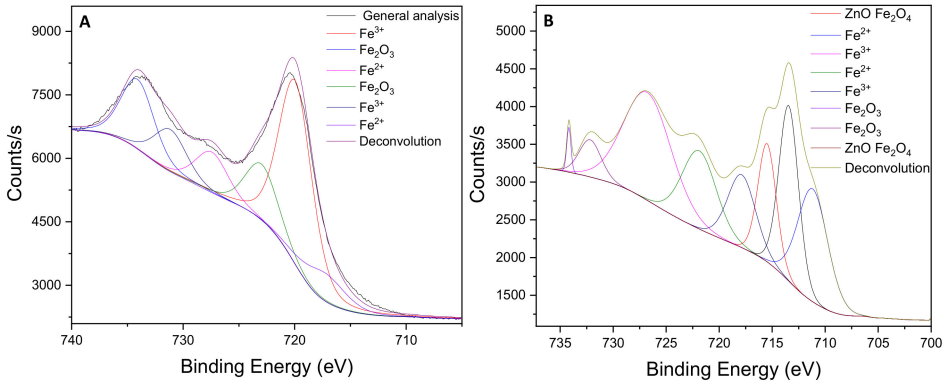

Figure 2. XPS spectra and corresponding fitting curves of (**A**) γ-/α-Fe_2O_3 and (**B**) γ-/α-Fe_2O_3/ZnO.

The morphology of nanoparticles was characterized by S/TEM. According to Figure 3A, the γ-/α-Fe_2O_3 material showed an aggregation of the nanowire shape, with a length between 125 to 330 nm and a diameter of 18 nm (see Figure S2). These nanostructures have been previously obtained by the precipitation method and calcinated between 400 °C to 600 °C in air [30,31], or by hydrothermal methods [32], high pressures, or using other chemical precursors [33,34]. In this sense, several forms such as spindle, ellipsoid, spherical, and quasi-cubic [33,34] have been previously reported.

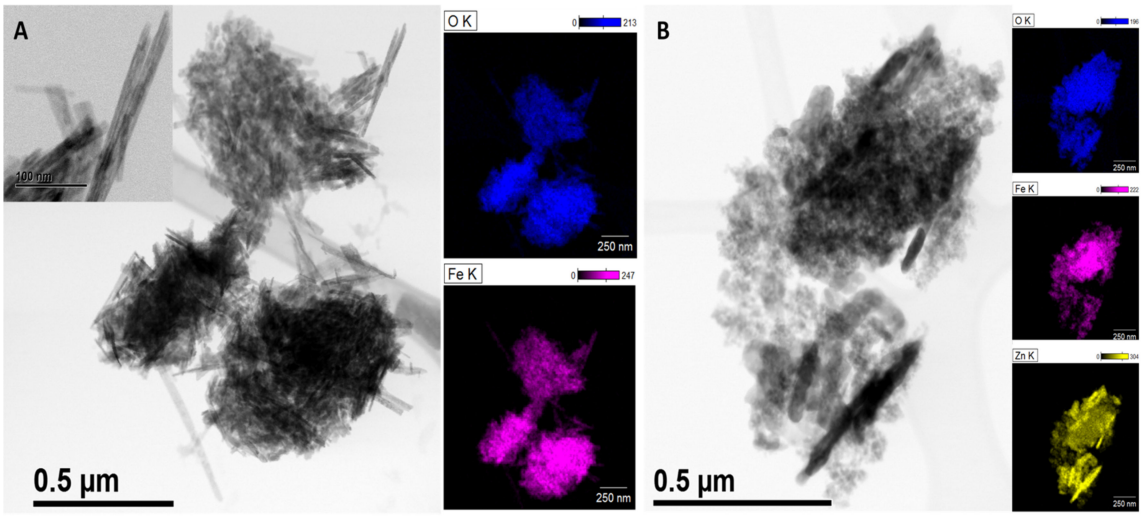

Figure 3. S/TEM and EDS mapping images of (**A**) γ-/α-Fe_2O_3 and (**B**) γ-/α-Fe_2O_3/ZnO nanoparticles.

The architecture of the γ-/α-Fe_2O_3/ZnO material consisted of a mixture of nanowires and spherical-shape nanoparticles with an average size of 15 to 18 nm (Figure 3B). EDS analysis evidenced an aggregation of Fe, Zn, and O, as well as a random distribution between Fe_2O_3 with ZnO. Several morphologies of the Fe_2O_3/ZnO material also synthesized by the precipitation method have been reported, such as flowers [35], microflowers, nanosheets [24,36–39], hexagonal [40], spheres [41,42], core-shell nanoparticles [43,44], nanorods core-shell configuration [41], and nanotubes [42].

3.2. Evaluation of Peroxidase-like Activity of γ-/α-Fe_2O_3 and γ-/α-Fe_2O_3/ZnO

The evaluation of the synthesized nanoparticles, e.g., peroxidases-like activity, was carried out by a UV-vis absorbance technique at 655 nm, chosen from a wavelength scan between 400 to 800 nm (Figure S3). The TMB concentration (500 μM) was obtained from the slope in the plot of absorbance as a function of the TMB concentration in the presence of 1 mM H_2O_2 (Figure S4). The resulting graphs as a function of the H_2O_2 concentration for each material γ-/α-Fe_2O_3 (Figure 4A) and γ-/α-Fe_2O_3/ZnO (Figure 4B) showed a typical Michaelis–Menten behavior, whereas the maximum velocity (Vmax) and Michaelis–Menten constant (Km) were calculated from Lineweaver–Burk plots. Km values of 0.02 mM and 0.03 mM were estimated by using γ-/α-Fe_2O_3 and γ-/α-Fe_2O_3/ZnO, respectively. In both cases, the results indicate that the synthesized materials have high affinity for the substrate compared to other iron-based nanoparticles [21]. Values of 6.0×10^{-8} M s^{-1} and 8.9×10^{-8} M s^{-1} for Vmax were obtained for γ-/α-Fe_2O_3 and γ-/α-Fe_2O_3/ZnO, respectively, indicating a faster reaction rate, possibly due to a higher dispersion of the Fe_2O_3 catalyst with the intercalation within ZnO. These results are compared with other works already published (Table 1), where the lowest calculated Km was 0.013 mM (0.65 times lower than that obtained in this work) [43], and 2.25×10^{-5} M s^{-1} was the highest Vmax [19]. The results show that when Fe_2O_3 is doped with some material, the Vmax increases (see Table 1). The same behavior is observed when the ZnO material is incorporated, even in the bi-phase γ-/α-Fe_2O_3 compared to the already reported Fe_3O_4 [17].

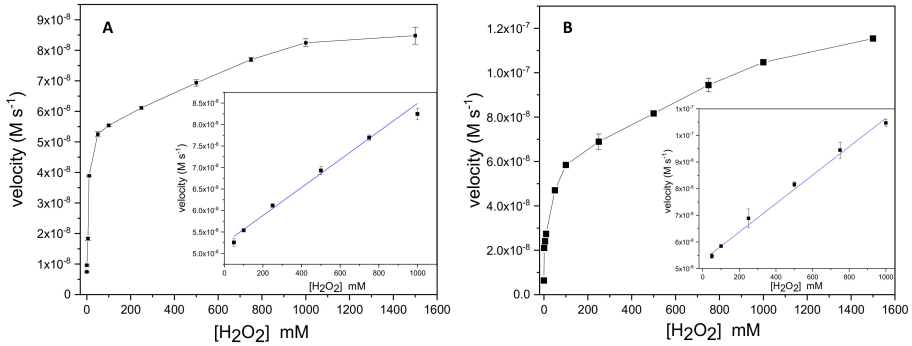

Figure 4. Steady-state kinetic assays of the (**A**) γ-/α-Fe_2O_3 and (**B**) γ-/α-Fe_2O_3/ZnO. TMB concentration was maintained in 500 μM and H_2O_2 concentration was varied. Insets are the linearity of steady-state curves.

Table 1. Comparison of Km and Vmax values of γ-/α-Fe_2O_3 and γ-/α-Fe_2O_3/ZnO.

Catalyst	Km (mM)	Vmax (M s^{-1})	Ref.
γ-/α-Fe_2O_3	0.02	6.0×10^{-8}	This work
γ-/α-Fe_2O_3/ZnO	0.03	8.9×10^{-8}	This work
Fe_3O_4@C	0.014	13.35×10^{-8}	[43]
Fe_3O_4	0.013	2.95×10^{-8}	[17]
H_2TCPP-γ-Fe_2O_3	0.013	21.14×10^{-9}	[17]
GO-Fe_2O_3	0.71	5.31×10^{-8}	[21]
γ-Fe_2O_3-SiO_2	0.63	2.25×10^{-5}	[19]
PB-Fe_2O_3	91.54	8.31×10^{-8}	[44]
$ZnFe_2O_4$	1.66	7.74×10^{-8}	[18]

From the H_2O_2 calibration curve, a linear range between 50–1000 μM (R^2 0.9956) was obtained using both nanoparticles, as well as 4.3 and 9.4 μM limits of detection (LOD) for γ-/α-Fe_2O_3 and γ-/α-Fe_2O_3/ZnO, respectively. The limits of quantification (LOQ) were estimated in 14.5 and 31.5 μM, respectively. This result is higher than those previously reported by other authors using iron oxides [16,20]. Likewise, colorimetric Au-Ag-based lactate sensors have reported LODs of 0.3 and 3 μM, whereas linear ranges are between 0.1–1000 μM, 0.8–90, and 90–500 μM. The results here obtained are comparable and, in some cases, higher, but with the advantage of using economically accessible materials [45]. The good activity, in terms of Km and Vmax values, obtained when γ-/α-Fe_2O_3 material was used could be attributed to the combination of both crystalline phases, which prevents the agglomeration and maximizes the reaction area.

3.3. Lactate Detection Using LOx, γ-/α-Fe_2O_3, and γ-/α-Fe_2O_3/ZnO

The nanoparticles of γ-/α-Fe_2O_3 and γ-/α-Fe_2O_3/ZnO combined with LOx were tested as a lactate sensor. For this procedure, it was assumed that the lactate oxidation reaction by LOx produces H_2O_2, which reacts with the TMB in the presence of the synthesized material, resulting in a color change that can be followed by UV-Vis spectroscopy. As can be seen in the upper part of Figure 5, a higher lactate concentration corresponds to a greater color intensity. The linear range for the lactate concentration was 50 to 1000 μM (R^2 0.9565) using both nanoparticles. The Km values estimated from the Lineweaver–Burk equation were 1.23 mM and 13.9 mM for γ-/α-Fe_2O_3 (Figure 5A) and γ-/α-Fe_2O_3/ZnO (Figure 5B), respectively. The LOD value was 50 μM for both nanomaterials. Already-published NPs have reported 0.0033 μM LOD and two linear ranges of 0.1–22 μM and 22–220 μM using noble metals, such as Au-Ag/C NC/LOx [45]. In the case of Ag/C, 0.35 μM LOD with two linear ranges of 1–30 μM and 30–900 μM was obtained [46]. Using Pt NPs, 0.6 μM LOD and a linear range of 2.5–100 μM were reported [47]. Hyun Jung Kim et al. reported 1 mM LOD and R^2 0.9684 using a paper-based colorimetric lactate sensor [48]. Though the LODs values are less than those obtained in this work, the range of detection is higher without the use of precious metals.

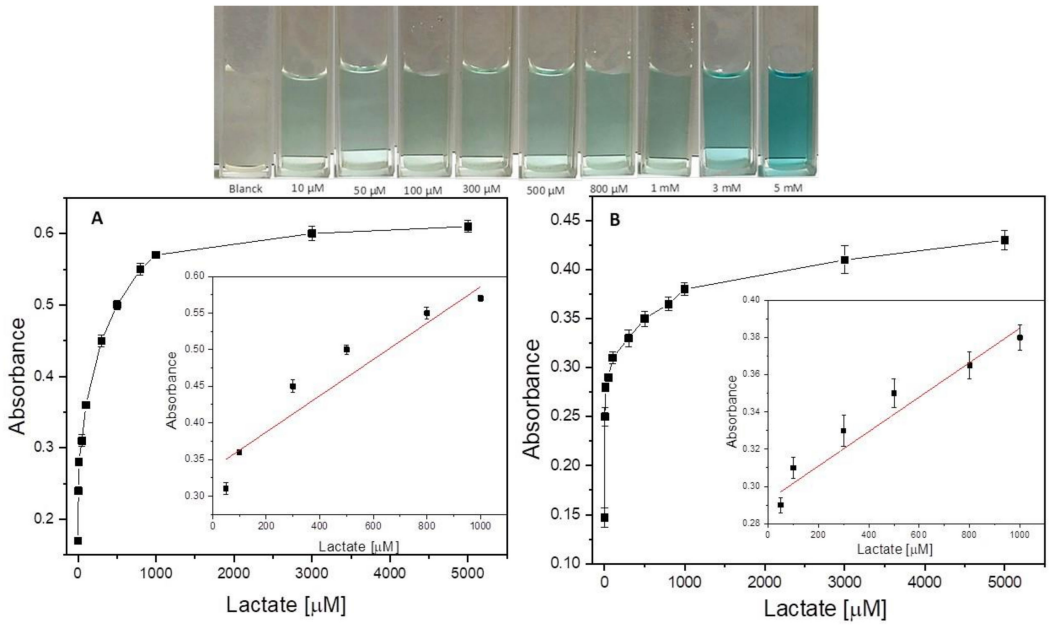

Figure 5. Lactate concentration–response curve using (**A**) LOx/TMB/γ-/α-Fe_2O_3 and (**B**) LOx/TMB/γ-/α-Fe_2O_3/ZnO system. Insets are the linear calibration of lactate response. Top color changes from lower to higher lactate concentrations.

Furthermore, in order to evaluate the selectivity of the lactate sensor, γ-/α-Fe_2O_3 and γ-/α-Fe_2O_3/ZnO NPs were evaluated in the presence of different interferents. As can be seen in Figure 6, the absorbance was measured at 1 mM lactate in the presence of 0.5 mM of molecules that could interfere in the lactate quantification in biological fluids, such as dopamine (DA), acid ascorbic (AA), uric acid (UA), glucose (Glu), urea, and cations, such as Ca^{2+} and Fe^{3+} [49]. Using both Nps did not influence the lactate detection due to the Lox specificity and selectivity; however, by using LOx/γ-/α-Fe_2O_3/ZnO, the standard deviation values were lower. This result could be attributed to ZnO, which acts as a quenched agent for Fe^{+3} and for organic molecules such as dopamine [50,51].

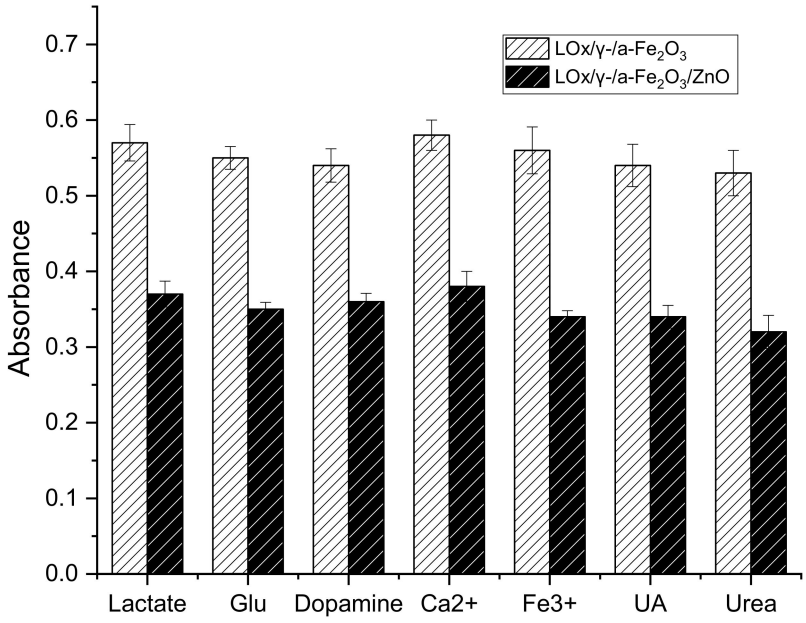

Figure 6. Selectivity of LOx/γ-/α-Fe_2O_3 and LOx/γ-/α-Fe_2O_3/ZnO NPs in the presence of lactate and interferents at 655 nm (pH 7.4).

After evaluating the catalytic activity of the NPs in the presence of lactate and their selectivity in the presence of some interferents, the characterization continued by using real serum samples. For this evaluation, blood serum samples were obtained from six volunteers, whose lactate concentration was measured using a blood serum meter, glucose/lactate Accutrend® Plus brand. Subsequently, applying the same method previously used in lactate detection, blood serum (200 µL) was measured at 653 nm after the incubation time. For the estimation of lactate concentration in serum samples, the equation of the straight line of the calibration curve was used using both NPs presented in Figure 4. The obtained values are shown in Table 2, where the results are compared with those obtained by using a commercial lactometer. The relative error values are greater when LOx/γ-/α-Fe_2O_3 was used compared to those values obtained with LOx/γ-/α-Fe_2O_3/ZnO. Finally, the obtained values of lactate concentration obtained by using the NPs synthesized in this work are comparable with those previously obtained by other authors in body fluids such as sweat [52,53] and blood [49,54,55]. A better fit in the linearity of the lactate sensor is important because it reduces measurement errors and is easier to calibrate. The reported linear range for lactate biosensors is suitable for the concentrations found in different biological fluids. For example, in blood, it is between 0.5–2.2 mM and reaches up to 15 mM in conditions of prolonged exercise or metabolic pathologies [56]. In tears, it can be found between 1–5 mM and 16–30 mM in sweat, reaching up to 120 mM under exhaustive exercise conditions [57,58].

Table 2. Comparison of lactate concentration values obtained from the calibration curve with those measurements using a commercial lactometer in human serum samples.

Sample	Estimated Lactate Concentration-mmol L^{-1}		Lactate Concentration-mmol L^{-1} (Lactometer)	Relative Error %	
	LOx/γ-/α-Fe_2O_3	LOx/γ-/α-Fe_2O_3/ZnO		LOx/γ-/α-Fe_2O_3	LOx/γ-/α-Fe_2O_3/ZnO
1	6.01	6.48	6.4	6.1	1.3
2	5.9	6.26	6.4	7.8	2.2
3	8.25	8.42	8.7	5.2	3.2
4	6.77	6.75	6.9	1.9	2.2
5	4.66	5.14	5.4	13.7	4.8
6	5.17	5.89	5.7	9.3	3.3

Although the tendency of actual sensors is the detection of lactate in sweat [59,60], colorimetric methods continue to be the simplest and most widely used. The results obtained here are promising due to more economical catalytic materials being used compared to those previously reported [45]. Furthermore, according to the difference of the isoelectronic point between ZnO and LOx of ~9.5 and 4.3, respectively [61], the presence of ZnO in the γ-/α-Fe_2O_3/ZnO structure could facilitate the LOx immobilization, whereas the Fe_2O_3-based nanomaterial allows the catalysis of H_2O_2, which means a synergetic contribution for the lactate colorimetric sensing. In this same sense, both nanoparticles evaluated are highly selective in the quantification of lactate in the presence of different biological interferents.

4. Conclusions

In this work, bi-phase γ-/α-Fe_2O_3 and γ-/α-Fe_2O_3/ZnO nanostructured materials were tested, e.g., peroxidase-like activity and lactate colorimetric sensors. The synthesis method was simple and economically accessible. Several physicochemical techniques, XRD, XPS and S/TEM, corroborated the structure and composition of the bi-phase nanoparticles. The proposed methodology in the presence of H_2O_2 indicated that γ-/α-Fe_2O_3 and γ-/α-Fe_2O_3/ZnO exhibit intrinsic peroxidase-like activity, whereas the kinetics and catalytic parameters evaluated by the Michaelis–Menten theory showed similar and superior values compared to those previously obtained with other iron oxide-based materials. The material based-on γ-/α-Fe_2O_3 presented a greater catalytic activity compared to other already-published peroxidase-like materials, whereas the γ-/α-Fe_2O_3/ZnO material retained its catalytic activity and exhibited a more stable signal. By a combination of synergetic properties of both metallic oxides (Fe_2O_3 and ZnO) using lactate oxidase enzyme, a cheap and simple lactate colorimetric sensor was constructed and evaluated using human serum samples with an acceptable quantification of lactate concentration compared to the values obtained with a commercial lactometer.

Supplementary Materials: The following supporting information can be downloaded at: https://www.mdpi.com/article/10.3390/bios12111025/s1, Figure S1. XPS spectra and corresponding fitting curves of γ-Fe_2O_3 (A), α-Fe_2O_3 (B), and ZnO (C); Figure S2. S/TEM images of the size of γ-/α-Fe_2O_3 (left) and γ-/α-Fe_2O_3/ZnO composite particles (right); Figure S3. Absorbance spectra of TMB–H_2O_2 of γ-/α-Fe_2O_3 (black line) and γ-/α-Fe_2O_3/ZnO (blue line) solutions. The reaction was performed in 1.9 mL NaHOAc buffer (0.01 M, pH 4.0), 30 µL of 500 µM TMB, 30 µL H_2O_2 at 30%, and 20 µL NPs (5 mg mL^{-1}); Figure S4. Plot of absorbance as a function of the concentration of TMB with 1 mM H_2O_2; Table S1. Zn/Fe/O and γ-Fe_2O_3:α-Fe_2O_3 ratio from γ-/α-Fe_2O_3/ZnO.

Author Contributions: Conceptualization, R.A.E.-V., K.V.-P., J.A.R.-M. and J.L.-G.; methodology, R.A.E.-V., K.V.-P., J.L.-G., L.G.A. and F.C.M.; software, F.C.M. and F.I.E.-L.; formal analysis, R.A.E.-V.,

F.I.E.-L., F.C.M., S.D.M. and J.L.-G.; investigation, R.A.E.-V., K.V.-P. and J.L.-G.; resources, J.L.-G., S.D.M. and L.G.A.; visualization, R.A.E.-V., F.I.E.-L. and F.C.M.; writing—original draft preparation, R.A.E.-V., K.V.-P. and J.L.-G.; writing—review and editing, R.A.E.-V., S.D.M., L.G.A. and J.L.-G.; supervision, R.A.E.-V., J.A.R.-M. and J.L.-G.; funding acquisition, J.L.-G. All authors have read and agreed to the published version of the manuscript.

Funding: The authors acknowledge the Mexican Council for Science and Technology (CONACYT) for financial support through project Ciencia de Frontera Grant no. 845132.

Institutional Review Board Statement: Not applicable.

Informed Consent Statement: Not applicable.

Data Availability Statement: Not applicable.

Acknowledgments: The authors acknowledge the CONACYT, UAQ and LABMyN 2023.

Conflicts of Interest: The authors declare no conflict of interest.

References

1. Kucherenko, I.S.; Topolnikova, Y.V.; Soldatkin, O.O. Advances in the Biosensors for Lactate and Pyruvate Detection for Medical Applications: A Review. *TrAC Trends Anal. Chem.* **2019**, *110*, 160–172. [CrossRef]
2. Heinemann, B. A Rapid Colorimetric Method for the Determination of Lactic Acid in Milk. *J. Dairy Sci.* **1940**, *23*, 969–972. [CrossRef]
3. Rathee, K.; Dhull, V.; Dhull, R.; Singh, S. Biosensors Based on Electrochemical Lactate Detection: A Comprehensive Review. *Biochem. Biophys. Rep.* **2016**, *5*, 35–54. [CrossRef] [PubMed]
4. Barker, S.B.; Summerson, W.H. The Colorimetric Determination of Lactic Acid in Biological Material. *J. Biol. Chem.* **1941**, *138*, 535–554. [CrossRef]
5. Rattu, G.; Murali Krishna, P. Enzyme-Free Colorimetric Nanosensor for the Rapid Detection of Lactic Acid in Food Quality Analysis. *J. Agric. Food Res.* **2022**, *7*, 100268. [CrossRef]
6. Harvey, C.J.; LeBouf, R.F.; Stefaniak, A.B. Formulation and Stability of a Novel Artificial Human Sweat under Conditions of Storage and Use. *Toxicol. In Vitro* **2010**, *24*, 1790–1796. [CrossRef]
7. Zhou, Y.; Han, H.; Naw, H.P.P.; Lammy, A.V.; Goh, C.H.; Boujday, S.; Steele, T.W.J. Real-Time Colorimetric Hydration Sensor for Sport Activities. *Mater. Des.* **2016**, *90*, 1181–1185. [CrossRef]
8. Petropoulos, K.; Piermarini, S.; Bernardini, S.; Palleschi, G.; Moscone, D. Development of a Disposable Biosensor for Lactate Monitoring in Saliva. *Sens. Actuators B Chem.* **2016**, *237*, 8–15. [CrossRef]
9. Deng, H.-H.; Li, G.-W.; Hong, L.; Liu, A.-L.; Chen, W.; Lin, X.-H.; Xia, X.-H. Colorimetric Sensor Based on Dual-Functional Gold Nanoparticles: Analyte-Recognition and Peroxidase-like Activity. *Food Chem.* **2014**, *147*, 257–261. [CrossRef]
10. Çelik, S.E.; Bekdeşer, B.; Apak, R. A Novel Colorimetric Sensor for Measuring Hydroperoxide Content and Peroxyl Radical Scavenging Activity Using Starch-Stabilized Gold Nanoparticles. *Talanta* **2019**, *196*, 32–38. [CrossRef]
11. Zhang, Y.; Zhang, Y.-J.; Xia, X.-D.; Hou, X.-Q.; Feng, C.-T.; Wang, J.-X.; Deng, L. A Quantitative Colorimetric Assay of H_2O_2 and Glucose Using Silver Nanoparticles Induced by H_2O_2 and UV. *Chin. Chem. Lett.* **2013**, *24*, 1053–1058. [CrossRef]
12. Chen, Z.; Zhang, C.; Wu, Q.; Li, K.; Tan, L. Application of Triangular Silver Nanoplates for Colorimetric Detection of H_2O_2. *Sens. Actuators B Chem.* **2015**, *220*, 314–317. [CrossRef]
13. Liu, S.; Lu, F.; Xing, R.; Zhu, J.-J. Structural Effects of Fe_3O_4 Nanocrystals on Peroxidase-like Activity. *Chem. A Eur. J.* **2011**, *17*, 620–625. [CrossRef] [PubMed]
14. Gao, L.; Zhuang, J.; Nie, L.; Zhang, J.; Zhang, Y.; Gu, N.; Wang, T.; Feng, J.; Yang, D.; Perrett, S.; et al. Intrinsic Peroxidase-like Activity of Ferromagnetic Nanoparticles. *Nat. Nanotechnol.* **2007**, *2*, 577–583. [CrossRef] [PubMed]
15. Puvvada, N.; Panigrahi, P.K.; Mandal, D.; Pathak, A. Shape Dependent Peroxidase Mimetic Activity towards Oxidation of Pyrogallol by H_2O_2. *RSC Adv.* **2012**, *2*, 3270–3273. [CrossRef]
16. Tan, Y.; Deng, W.; Ge, B.; Xie, Q.; Huang, J.; Yao, S. Biofuel Cell and Phenolic Biosensor Based on Acid-Resistant Laccase–Glutaraldehyde Functionalized Chitosan–Multiwalled Carbon Nanotubes Nanocomposite Film. *Biosens. Bioelectron.* **2009**, *24*, 2225–2231. [CrossRef]
17. Liu, Q.; Zhang, L.; Li, H.; Jia, Q.; Jiang, Y.; Yang, Y.; Zhu, R. One-Pot Synthesis of Porphyrin Functionalized γ-Fe_2O_3 Nanocomposites as Peroxidase Mimics for H_2O_2 and Glucose Detection. *Mater. Sci. Eng. C* **2015**, *55*, 193–200. [CrossRef]
18. Su, L.; Feng, J.; Zhou, X.; Ren, C.; Li, H.; Chen, X. Colorimetric Detection of Urine Glucose Based $ZnFe_2O_4$ Magnetic Nanoparticles. *Anal. Chem.* **2012**, *84*, 5753–5758. [CrossRef]
19. Lu, C.; Liu, X.; Li, Y.; Yu, F.; Tang, L.; Hu, Y.; Ying, Y. Multifunctional Janus Hematite–Silica Nanoparticles: Mimicking Peroxidase-like Activity and Sensitive Colorimetric Detection of Glucose. *ACS Appl. Mater. Interfaces* **2015**, *7*, 15395–15402. [CrossRef]
20. Shetti, N.P.; Bukkitgar, S.D.; Reddy, K.R.; Reddy, C.V.; Aminabhavi, T.M. ZnO-Based Nanostructured Electrodes for Electrochemical Sensors and Biosensors in Biomedical Applications. *Biosens. Bioelectron.* **2019**, *141*, 111417. [CrossRef]

21. Dong, Y.; Zhang, H.; Rahman, Z.U.; Su, L.; Chen, X.; Hu, J.; Chen, X. Graphene Oxide–Fe_3O_4 Magnetic Nanocomposites with Peroxidase-like Activity for Colorimetric Detection of Glucose. *Nanoscale* **2012**, *4*, 3969–3976. [CrossRef]
22. Ming, J.; Wu, Y.; Wang, L.; Yu, Y.; Zhao, F. CO_2-Assisted Template Synthesis of Porous Hollow Bi-Phase γ-/α-Fe_2O_3 Nanoparticles with High Sensor Property. *J. Mater. Chem.* **2011**, *21*, 17776–17782. [CrossRef]
23. Ma, Y.; Wang, B.; Wang, Q.; Xing, S. Facile Synthesis of α-FeOOH/γ-Fe_2O_3 by a PH Gradient Method and the Role of γ-Fe_2O_3 in H_2O_2 Activation under Visible Light Irradiation. *Chem. Eng. J.* **2018**, *354*, 75–84. [CrossRef]
24. Shooshtari, N.M.; Ghazi, M.M. An Investigation of the Photocatalytic Activity of Nano α-Fe_2O_3/ZnO on the Photodegradation of Cefixime Trihydrate. *Chem. Eng. J.* **2017**, *315*, 527–536. [CrossRef]
25. Langford, J.I.; Wilson, A.J.C. Scherrer after Sixty Years: A Survey and Some New Results in the Determination of Crystallite Size. *J. Appl. Crystallogr.* **1978**, *11*, 102–113. [CrossRef]
26. Hong, M.; Su, Y.; Zhou, C.; Yao, L.; Hu, J.; Yang, Z.; Zhang, L.; Zhou, Z.; Hu, N.; Zhang, Y. Scalable Synthesis of γ-Fe_2O_3/CNT Composite as High-Performance Anode Material for Lithium-Ion Batteries. *J. Alloys Compd.* **2019**, *770*, 116–124. [CrossRef]
27. Flak, D.; Chen, Q.; Mun, B.S.; Liu, Z.; Rękas, M.; Braun, A. In Snanoparticlesitu Ambient Pressure XPS Observation of Surface Chemistry and Electronic Structure of α-Fe_2O_3 and γ-Fe_2O_3. *Appl. Surf. Sci.* **2018**, *455*, 1019–1028. [CrossRef]
28. Zhao, D.; Xiao, Y.; Wang, X.; Gao, Q.; Cao, M. Ultra-High Lithium Storage Capacity Achieved by Porous $ZnFe_2O_4$/α-Fe_2O_3 Micro-Octahedrons. *Nano Energy* **2014**, *7*, 124–133. [CrossRef]
29. Yao, J.; Yan, J.; Huang, Y.; Li, Y.; Xiao, S.; Xiao, J. Preparation of $ZnFe_2O_4$/α-Fe_2O_3 Nanocomposites from Sulfuric Acid Leaching Liquor of Jarosite Residue and Their Application in Lithium-Ion Batteries. *Front. Chem.* **2018**, *6*, 442. [CrossRef]
30. Li, X.Q.; Li, D.P.; Xu, J.C.; Han, Y.B.; Jin, H.X.; Hong, B.; Ge, H.L.; Wang, X.Q. Calcination-Temperature-Dependent Gas-Sensing Properties of Mesoporous α-Fe_2O_3 Nanowires as Ethanol Sensors. *Solid State Sci.* **2017**, *69*, 38–43. [CrossRef]
31. Huang, B.; Tai, K.; Dillon, S.J. Structural Evolution of α-Fe_2O_3 Nanowires during Lithiation and Delithiation. *J. Power Sources* **2014**, *245*, 308–314. [CrossRef]
32. Xie, X.; Yang, Y.; Xiao, Y.-H.; Huang, X.; Shi, Q.; Zhang, W.-D. Enhancement of Photoelectrochemical Activity of Fe_2O_3 Nanowires Decorated with Carbon Quantum Dots. *Int. J. Hydrog. Energy* **2018**, *43*, 6954–6962. [CrossRef]
33. Chen, X.; Zhang, Z.; Qiu, Z.; Shi, C.; Li, X. A Facile Biomolecule-Assisted Approach for Fabricating α-Fe_2O_3 Nanowires in Solution. *Solid State Commun.* **2006**, *140*, 267–269. [CrossRef]
34. Tadic, M.; Trpkov, D.; Kopanja, L.; Vojnovic, S.; Panjan, M. Hydrothermal Synthesis of Hematite (α-Fe_2O_3) Nanoparticle Forms: Synthesis Conditions, Structure, Particle Shape Analysis, Cytotoxicity and Magnetic Properties. *J. Alloys Compd.* **2019**, *792*, 599–609. [CrossRef]
35. Xie, J.; Zhang, L.; Li, M.; Hao, Y.; Lian, Y.; Li, Z.; Wei, Y. α-Fe_2O_3 Modified ZnO Flower-like Microstructures with Enhanced Photocatalytic Performance for Pentachlorophenol Degradation. *Ceram. Int.* **2015**, *41*, 9420–9425. [CrossRef]
36. Bu, X.; Liu, F.; Zhang, Z.; Wang, Z.; Liu, J.; Liu, W. Facile Synthesis of Flower-like ZnO@Fe_2O_3 Hierarchical Nanostructures with Enhanced Catalytic Activity on the Thermal Decomposition of Ammonium Perchlorate. *Mater. Lett.* **2018**, *219*, 33–36. [CrossRef]
37. Huang, L.; Fan, H. Room-Temperature Solid State Synthesis of ZnO/α-Fe_2O_3 Hierarchical Nanostructures and Their Enhanced Gas-Sensing Properties. *Sens. Actuators B Chem.* **2012**, *171–172*, 1257–1263. [CrossRef]
38. Fu, R.; Wang, W.; Han, R.; Chen, K. Preparation and Characterization of γ-Fe_2O_3/ZnO Composite Particles. *Mater. Lett.* **2008**, *62*, 4066–4068. [CrossRef]
39. Yan, W.; Fan, H.; Yang, C. Ultra-Fast Synthesis and Enhanced Photocatalytic Properties of Alpha-Fe_2O_3/ZnO Core-Shell Structure. *Mater. Lett.* **2011**, *65*, 1595–1597. [CrossRef]
40. Typek, J.; Wardal, K.; Zolnierkiewicz, G.; Guskos, N.; Sibera, D.; Narkiewicz, U. Magnetic Study of 0.20(Fe_2O_3)/0.80(ZnO) Nanocomposite. *J. Magn. Magn. Mater.* **2014**, *361*, 12–18. [CrossRef]
41. Si, S.; Li, C.; Wang, X.; Peng, Q.; Li, Y. Fe2O3/ZnO Core–Shell Nanorods for Gas Sensors. *Sens. Actuators B Chem.* **2006**, *119*, 52–56. [CrossRef]
42. Liu, Y.; Sun, L.; Wu, J.; Fang, T.; Cai, R.; Wei, A. Preparation and Photocatalytic Activity of ZnO/Fe_2O_3 Nanotube Composites. *Mater. Sci. Eng. B* **2015**, *194*, 9–13. [CrossRef]
43. Li, Q.; Tang, G.; Xiong, X.; Cao, Y.; Chen, L.; Xu, F.; Tan, H. Carbon Coated Magnetite Nanoparticles with Improved Water-Dispersion and Peroxidase-like Activity for Colorimetric Sensing of Glucose. *Sens. Actuators B Chem.* **2015**, *215*, 86–92. [CrossRef]
44. Dutta, A.K.; Maji, S.K.; Biswas, P.; Adhikary, B. New Peroxidase-Substrate 3,5-Di-Tert-Butylcatechol for Colorimetric Determination of Blood Glucose in Presence of Prussian Blue-Modified Iron Oxide Nanoparticles. *Sens. Actuators B Chem.* **2013**, *177*, 676–683. [CrossRef]
45. Zhang, L.; Hou, W.; Lu, Q.; Liu, M.; Chen, C.; Zhang, Y.; Yao, S. Colorimetric Detection of Hydrogen Peroxide and Lactate Based on the Etching of the Carbon Based Au-Ag Bimetallic Nanocomposite Synthesized by Carbon Dots as the Reductant and Stabilizer. *Anal. Chim. Acta* **2016**, *947*, 23–31. [CrossRef]
46. Hou, W.; Liu, X.; Lu, Q.; Liu, M.; Zhang, Y.; Yao, S. Etching and Anti-Etching Strategy for Sensitive Colorimetric Sensing of H_2O_2 and Biothiols Based on Silver/Carbon Nanomaterial. *Colloids Surf. B Biointerfaces* **2018**, *162*, 118–125. [CrossRef]
47. Su, C.K.; Li, T.W.; Sun, Y.C. Peroxidase-Mimicking PtNP-Coated, 3D-Printed Multi-Well Plate for Rapid Determination of Glucose and Lactate in Clinical Samples. *Sens. Actuators B Chem.* **2018**, *269*, 46–53. [CrossRef]
48. Kim, H.; Park, I.; Pack, S.; Lee, G.; Hong, Y. Colorimetric Sensing of Lactate in Human Sweat Using Polyaniline Nanoparticles-Based Sensor Platform and Colorimeter. *Biosensors* **2022**, *12*, 248. [CrossRef] [PubMed]

49. Mirzaei, Y.; Gholami, A.; Bordbar, M.M. A Distance-Based Paper Sensor for Rapid Detection of Blood Lactate Concentration Using Gold Nanoparticles Synthesized by Satureja Hortensis. *Sens. Actuators B Chem.* **2021**, *345*, 130445. [CrossRef]
50. Alipour, N.; Namazi, H. Chelating ZnO-Dopamine on the Surface of Graphene Oxide and Its Application as PH-Responsive and Antibacterial Nanohybrid Delivery Agent for Doxorubicin. *Mater. Sci. Eng. C* **2020**, *108*, 110459. [CrossRef]
51. Seddik, B.; Salima, B.; Houda, G. Fe Doped ZnO Nanostructures Prepared via Sol-Gel Dip-Coating Technique for Iso-Butane (i-C4H10) Sensing. *Mater. Today Commun.* **2021**, *29*, 102805. [CrossRef]
52. Yüzer, E.; Doğan, V.; Kılıç, V.; Şen, M. Smartphone Embedded Deep Learning Approach for Highly Accurate and Automated Colorimetric Lactate Analysis in Sweat. *Sens. Actuators B Chem.* **2022**, *371*, 132489. [CrossRef]
53. Shitanda, I.; Mitsumoto, M.; Loew, N.; Yoshihara, Y.; Watanabe, H.; Mikawa, T.; Tsujimura, S.; Itagaki, M.; Motosuke, M. Continuous Sweat Lactate Monitoring System with Integrated Screen-Printed Mgo-Templated Carbon-Lactate Oxidase Biosensor and Microfluidic Sweat Collector. *Electrochim. Acta* **2021**, *368*, 137620. [CrossRef]
54. Zhu, D.D.; Zheng, L.W.; Duong, P.K.; Cheah, R.H.; Liu, X.Y.; Wong, J.R.; Wang, W.J.; Tien Guan, S.T.; Zheng, X.T.; Chen, P. Colorimetric Microneedle Patches for Multiplexed Transdermal Detection of Metabolites. *Biosens. Bioelectron.* **2022**, *212*, 114412. [CrossRef] [PubMed]
55. Yang, S.; Lu, F.; Liu, Y.; Ning, Y.; Tian, S.; Zuo, P.; Ji, X.; He, Z. Quantum Dots-Based Hydrogel Microspheres for Visual Determination of Lactate and Simultaneous Detection Coupled with Microfluidic Device. *Microchem. J.* **2021**, *171*, 106801. [CrossRef]
56. Mengarda, P.; Dias, F.A.L.; Peixoto, J.V.C.; Osiecki, R.; Bergamini, M.F.; Marcolino-Junior, L.H. Determination of Lactate Levels in Biological Fluids Using a Disposable Ion-Selective Potentiometric Sensor Based on Polypyrrole Films. *Sens. Actuators B Chem.* **2019**, *296*, 126663. [CrossRef]
57. Derbyshire, P.J.; Barr, H.; Davis, F.; Higson, S.P.J. Lactate in Human Sweat: A Critical Review of Research to the Present Day. *J. Physiol. Sci.* **2012**, *62*, 429–440. [CrossRef]
58. Lin, C.E.; Hiraka, K.; Matloff, D.; Johns, J.; Deng, A.; Sode, K.; La Belle, J. Development toward a Novel Integrated Tear Lactate Sensor Using Schirmer Test Strip and Engineered Lactate Oxidase. *Sens. Actuators B Chem.* **2018**, *270*, 525–529. [CrossRef]
59. Zhao, Z.; Li, Q.; Dong, Y.; Gong, J.; Li, Z.; Zhang, J. Core-Shell Structured Gold Nanorods on Thread-Embroidered Fabric-Based Microfluidic Device for Ex Situ Detection of Glucose and Lactate in Sweat. *Sens. Actuators B Chem.* **2022**, *353*, 131154. [CrossRef]
60. Promphet, N.; Rattanawaleedirojn, P.; Siralertmukul, K.; Soatthiyanon, N.; Potiyaraj, P.; Thanawattano, C.; Hinestroza, J.P.; Rodthongkum, N. Non-Invasive Textile Based Colorimetric Sensor for the Simultaneous Detection of Sweat PH and Lactate. *Talanta* **2019**, *192*, 424–430. [CrossRef]
61. Ogata, K.; Dobashi, H.; Koike, K.; Sasa, S.; Inoue, M.; Yano, M. Patterned Growth of ZnO Nanorods and Enzyme Immobilization toward the Fabrication of Glucose Sensors. *Phys. E Low-Dimens. Syst. Nanostruct.* **2010**, *42*, 2880–2883. [CrossRef]